Section 1 The supplementary Tables and Figures in the manuscript.

Table S1. Model scenarios used for gas-phase Mgly.

Model scenarios	Description
INITIAL	Default MCMv3.2, without considering the reversible and irreversible uptake of Mgly and the gas-particle partitioning of other oxidation products.
Scenario M1	As INITIAL, and considers Mgly partitions into the liquid-phase, without considering the monomers pool 1 and oligomers pool 2.
Scenario M2	As Scenario M1, and considers surface uptake by aerosols of Mgly with the uptake coefficient of 2.6×10^{-4}(Pye et al., 2017).

Table S2. Estimated uncertainties of model reaction rate constant and input parameters.

Input parameter	Uncertainty factor
j[a]	×1.1
τD	×2
T	×1.005
P	×1.005
OH	×1.2
H_2	×1.2
CO	×1.05
NO	×1.07
NO_2	×1.13
O_3	×1.05
H_2O	×1.1
HONO	×1.1
CH_4	×1.04
Ethane [b]	+0.2 ppb
Ethene [b]	+0.7 ppb
Ethyne [b]	+1.2 ppb
C3-C12 NMHCs	×1.2
K_i [C]	×1.3

[a] The errors of the measured photolysis frequencies are assumed to be correlated since they were derived from the same measurement of the solar actinic flux. [b] Campaign averaged values were applied for ethane, ethene, and ethyne, so that the standard deviation of the canister samples were propagated as uncertainties rather than the measurement accuracy. [c] All the reaction constants of non-photolytic reactions in MCM v3.2 are estimated to have 30% accuracy (1σ)(Li et al., 2014; Lu et al., 2012).

Table S3 the sensitivity test of physical processes

	Gly			Mgly		
time	INITIAL[a]	Dry depsition[b]	Duiltion[c]	INITIAL[a]	Dry deposition[b]	Dilution[c]
6:00	0.004	0.004	0.004	0.005	0.005	0.005
7:00	0.017	0.017	0.016	0.021	0.021	0.020
8:00	0.036	0.036	0.032	0.047	0.046	0.045
9:00	0.072	0.071	0.067	0.092	0.092	0.088
10:00	0.140	0.138	0.128	0.180	0.177	0.169
11:00	0.224	0.220	0.206	0.311	0.307	0.291
12:00	0.309	0.300	0.284	0.449	0.420	0.419
13:00	0.364	0.354	0.332	0.509	0.500	0.473
14:00	0.400	0.392	0.367	0.541	0.531	0.498
15:00	0.393	0.379	0.359	0.501	0.490	0.459
16:00	0.373	0.359	0.339	0.455	0.442	0.416
17:00	0.376	0.361	0.340	0.441	0.430	0.400
18:00	0.365	0.350	0.322	0.424	0.410	0.384
19:00	0.353	0.336	0.314	0.406	0.390	0.367

[a] Data modeled from the INITIAL scenario.

[b] Based on the INITIAL scenario, the dry deposition rate multiplied by two for Gly/Mgly modeled.

[c] Based on the INITIAL scenario, the dilution rate multiplied by two for Gly/Mgly modeled.

Table S4. Absolute and relative changes of Gly mixing ratio, and the contribution of differ aerosol sinks to total heterogeneous loss of Gly under different model simulations for the Heshan site. When the model scenario is changing from A to B, the absolute changes of Gly mixing ratio is calculated as $\triangle Gly = B - A$; the relative change in percentage is calculated as $\% = 100\times \triangle Gly / A$.

Scenario	Time period	Relative change in Gly %
INITIAL → scenario 1	06-12	-1.70%
	13-19	-0.60%
	06-19	-1.20%
Scenario 1 → scenario 2	06-12	-1.40%
	13-19	-2.40%
	06-19	-1.90%
Scenario 2 → scenario 3	06-12	-17.3%
	13-19	-34.0%
	06-19	-25.7%
Scenario 3 → scenario 4	06-12	-55.0%
	13-19	-68.4%
	06-19	-61.7%
INITIAL → scenario 4	06-12	-65.0%
	13-19	-79.6%
	06-19	-72.3%

Table S5. Absolute and relative changes of Mgly mixing ratio, and the contribution of differ aerosol sinks to total heterogeneous loss of Mgly under different model simulations for the Heshan site. When the model scenario is changing from A to B, the absolute changes of Mgly mixing ratio is calculated as $\triangle Mgly = B - A$; the relative change in percentage is calculated as $\% = 100\times \triangle Mgly / A$.

scenario	Time period	Relative change in Mgly %
INITIAL → scenario M1	06-12	-46.0%
	13-19	-36.7%
	06-19	-41.3%
Scenario M1 → scenario M2	06-12	-50.5%
	13-19	-60.9%
	06-19	-55.7%
INITIAL → scenario M2	06-12	-61.4%
	13-19	-82.6%
	06-19	-73.0%

Table S6. Comparison of the results from this work and previous researches in PRD

	This study								Li Nan's study			
	Gly		Mgly		Gly		Mgly		Gly		Mgly	
	γ^a= 1×10^{-3}				γ = 2.9×10^{-3}				γ = 2.9×10^{-3}			
	SOA[b]	% [c]	SOA	%	SOA	%	SOA	%	SOA	%	SOA	%
m,p-Xylene	0.063	2.6%	0.081	3.3%	0.55 0.64[d]	8.0% 9.4%	0.56 0.81	8.2% 11.8%	0.20	2.2%	0.23	2.5%
o-Xylene	0.023	0.93 %	0.014	0.57%	0.18 0.19	2.6% 2.8%	0.09 0.13	1.3% 1.9%				
Toluene	0.079	3.2%	0.019	0.77%	0.63 0.77	9.2% 11%	0.13 0.19	1.9% 2.8%	0.16	1.8%	0.07	0.77%
SOA_{het}	0.28	11%	0.25	10%	2.1 2.5	31% 37%	2.0 2.4	29% 35%	2.33	26%	2.51	27%

[a] Uptake coefficients.
[b] Unit: ug/m^3.
[c] The contribution to the total SOA (i.e., scenario 4).
[d] Solely a surface uptake process for aerosol sink marked in red.

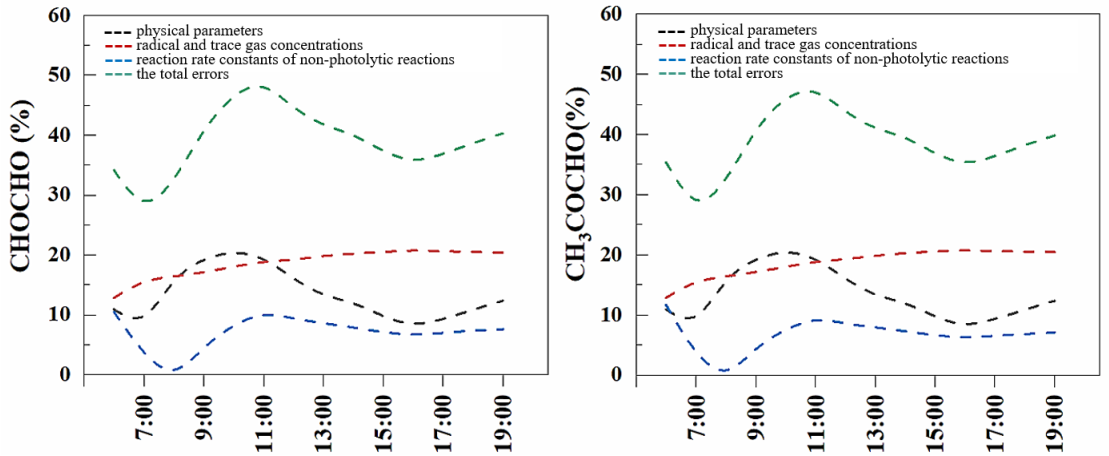

Figure S1. Mean diurnal variation of the uncertainty of the Gly and Mgly concentrations predicted by $MCM_v3.2$ model.

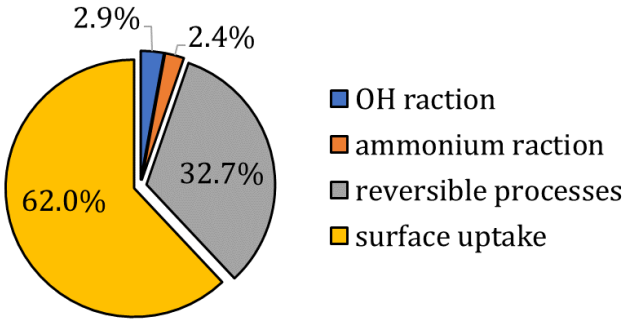

Figure S2. the contribution of differ aerosol sinks is calculated under the scenario 4.

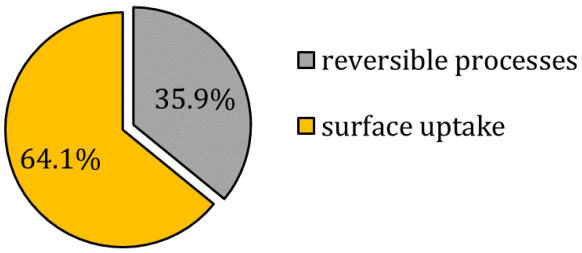

Figure S3. the contribution of differ aerosol sinks is calculated under the scenario M2.

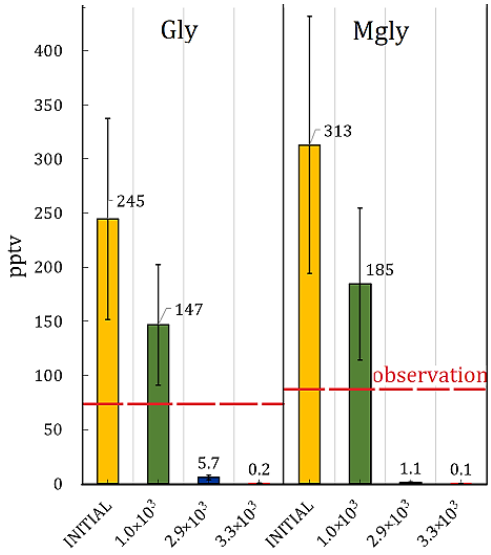

Figure S4. the daily average concentration of Gly and Mgly predicted from INITIAL and surface uptake scenarios (i.e., as INITIAL, and considers surface uptake by aerosols of Mgly and Mgly with the uptake coefficient of 1.0×10^{3}, 2.9×10^{3}, 3.3×10^{3}, respectively).

Section 2. The definition and configuration of each parameter used in equations 4-8

The reversible partitioning of Gly and Mgly on aerosols aqueous phase is usually described by the Henry's law equilibrium (Kampf et al., 2013) (Eq.4):

$$[Gly(Mgly)]_{liquid} = K_H \times [Gly(Mgly)]_{gas} \quad \text{(Eq.4)}$$

where $[Gly(Mgly)]_{liquid}$ and the $[Gly(Mgly)]_{gas}$ denote the concentration of Gly and Mgly in liquid-phase and gas-phase, respectively, whereas K_H (mol L^{-1} atm^{-1}) represents the Henry's law coefficient. Recently laboratorial studies had indicated that hydration of carbonyls function groups and salt-Gly interactions could have significant influences on the K_H value of Gly (Kampf et al., 2013; Waxman et al., 2015). Thus, an effective Henry's law coefficient expressed by Eq.5 was often used.

$$K_{H,effective} = \frac{K_{H,water}}{10^{(-0.24\min(12.0,(C_{as}+C_{an}))}} \quad \text{(Eq.5)}$$

where $K_{H,water}$ represents the henry's law constant of Gly observed for water, with value of 4.19×10^5 M atm^{-1} (Knote et al., 2014). -0.24 is the "salting–in" constant of ammonium sulfate and nitrate (Kampf et al., 2013; Waxman et al., 2015). The concentrations of ammonium sulfate and nitrate are defined as C_{as}(M) and C_{an}(M), respectively. Furthermore, it was suggested that a low increase of $K_{H,effective}$ could be found at high concentrations of ammonium sulfate and nitrate (*i.e.,* 12 M) within the time scales of their experiments (*i.e.,* 60×10^3 s), while the equilibrium for Gly partitioning could be reached rapidly when the concentrations of ammonium sulfate and nitrate were lower (*i.e.,* < 12 M) (Kampf et al., 2013).

As variations were found for the value of $K_{H,effective}$ under different concentrations of ammonium sulfate and nitrate in previous studies (Erverns and Volkamer, 2010; Knote et al., 2014; Kampf et al., 2013), we calculated this vital parameter (*i.e.,* C_{as} + C_{an} for each hour in the present study. The C_{as} and C_{an} were calculated from the measured ammonium sulfate (or ammonium nitrate) concentrations (mol m^{-3}) divided by aerosol liquid water content (ALWC, kg m^{-3}), which were determined by the aerosol inorganics model (AIM-IV, http://www.aim.env.uea.ac.uk/aim/model4/model4a.php)

with inputs of the observed parameters (*e.g.*, ambient relative humidity, temperature, and the moles of each ion) at the Heshan site (Chang et al., 2019).

The reversible formation of monomer (*i.e.*, glyoxal, glyoxal monohydrate, and glyoxal dihydrate) and oligomers are considered with the two important reservoirs (*i.e.,* monomer and oligomer pools, represented as pool1 and pool2 in Knote et al. (2014)). The variations of the glyoxal monomer ([Gly_{p1}]) and oligomer concentrations ([Gly_{p2}]) with time can be represented based on Erverns and Volkamer, (2010), Kampf et al. (2013) and Knote et al. (2014), as follows:

$$\frac{d([Gly_{p1}])}{dt} = \frac{1}{\tau_1} \times (Gly_{p1,eq} - Gly_{p1}) \text{ (Eq.6)}$$

$$\frac{d([Gly_{p2}])}{dt} = \frac{1}{\tau_2} \times (Gly_{p2,eq} - Gly_{p2}) \text{ (Eq.7)}$$

$$\frac{Gly_{p2,eq}}{Gly_{p1,eq}} = K_{olig} \text{ (Eq.8)}$$

Where Gly_{p1} and Gly_{p2} were the current concentrations of Gly in monomers and oligomers pool, respectively. $Gly_{p1,eq}$ and $Gly_{p2,eq}$ were the concentrations in each pool at equilibrium, while τ_1 and τ_2 were the characteristic time scales to fill the monomer/oligomer pools, respectively.

References

Chang, D., Wang, Z., Guo, J., Li, T., Liang, Y. H., Kang, L. Y., Xia, M., Wang, Y., Yu, C., Yun, H., Yue, D. L., Wang, T., 2019. Characterization of organic aerosols and their precursors in southern China during a severe haze episode in January 2017. Sci. Total Environ. 691, 101-111.

Ervens, B. and Volkamer, R., 2010. Glyoxal processing by aerosol multiphase chemistry: towards a kinetic modeling framework of secondary organic aerosol formation in aqueous particles. Atmospheric Chemistry and Physics. 1017, 8219-8244.

Kampf, C. J. , Waxman, E. M. , Slowik, J. G. , Dommen, J. , Pfaffenberger, L. , Praplan, A. P. , André SH, Baltensperger, U, Hoffmann, T, Volkamer, R., 2013. Effective Henry's law partitioning and the salting constant of glyoxal in aerosols containing sulfate. Environ. Sci. Technol. 47(9), 4236-4244.

Knote, C., Hodzic, A., Jimenez, JL, Volkamer, R., Orlando, JJ, Baidar, S, Brioude, J, Fast, J, Gentner, DR, Goldstein, AH. 2014. Simulation of semi-explicit mechanisms of SOA formation from glyoxal in aerosol in a 3-D model. Atmos. Chem. Phys. 1412, 6213-6239.

Li, X., Rohrer, F., Brauers, T., Hofzumahaus, A., Wahner, A., 2014. Modeling of HCHO and

CHOCHO at a semi-rural site in southern China during the PRIDE-PRD2006 campaign. Atmos. Chem. Phys. 14(22), 33013-33054.

Lu, K. D., Rohrer, F., Holland, F., Fuchs, H., Bohn, B., Brauers, T., Chang, C. C., Häseler, R., Hu, M., Kita, K., Kondo, Y., Li, X., Lou, S. R., Nehr, S., Shao, M., Zeng, L. M., Wahner, A., Zhang, Y. H., Hofzumahaus, A., 2012. Observation and modelling of OH and HO2 concentrations in the Pearl River Delta 2006: a missing OH source in a VOC rich atmosphere. Atmos. Chem. Phys. 12(3), 1541-1569.

Pye, H. O. T., Murphy, B. N., Xu, L. , Ng, N. L., Carlton, A. G., Guo, H., 2017. On the implications of aerosol liquid water and phase separation for organic aerosol mass. Atmos. Chem. Phys. 17(1), 343-369.

Waxman, E. M., Elm, J., Kurtén, T., Mikkelsen, K. V., Ziemann, P. J., Volkamer, R., 2015. Glyoxal and methylglyoxal setschenow salting constants in sulfate, nitrate, and chloride solutions: Measurements and Gibbs energies. Environ. Sci. Technol. 4919, 11500-11508.